Citation: Molecular Therapy—Nucleic Acids (2014) 3, e159; doi:10.1038/mtna.2014.9

www.nature.com/mtna

Silencing VDAC1 Expression by siRNA Inhibits Cancer Cell Proliferation and Tumor Growth *In Vivo*

Tasleem Arif[1], Lilia Vasilkovsky[1], Yael Refaely[2], Alexander Konson[1] and Varda Shoshan-Barmatz[1]

Alterations in cellular metabolism and bioenergetics are vital for cancer cell growth and motility. Here, the role of the mitochondrial protein voltage-dependent anion channel (VDAC1), a master gatekeeper regulating the flux of metabolites and ions between mitochondria and the cytoplasm, in regulating the growth of several cancer cell lines was investigated by silencing VDAC1 expression using small interfering RNA (siRNA). A single siRNA specific to the human VDAC1 sequence at nanomolar concentrations led to some 90% decrease in VDAC1 levels in the lung A549 and H358, prostate PC-3, colon HCT116, glioblastoma U87, liver HepG2, and pancreas Panc-1 cancer cell lines. VDAC1 silencing persisted 144 hours post-transfection and resulted in profound inhibition of cell growth in cancer but not in noncancerous cells, with up to 90% inhibition being observed over 5 days that was prolonged by a second transfection. Cells expressing low VDAC1 levels showed decreased mitochondrial membrane potential and adenoside triphosphate (ATP) levels, suggesting limited metabolite exchange between mitochondria and cytosol. Moreover, cells silenced for VDAC1 expression showed decreased migration, even in the presence of the wound healing accelerator basic fibroblast growth factor (bFGF). VDAC1-siRNA inhibited cancer cell growth in a Matrigel-based assay in host nude mice. Finally, in a xenograft lung cancer mouse model, chemically modified VDAC1-siRNA not only inhibited tumor growth but also resulted in tumor regression. This study thus shows that VDAC1 silencing by means of RNA interference (RNAi) dramatically inhibits cancer cell growth and tumor development by disabling the abnormal metabolic behavior of cancer cells, potentially paving the way for a more effective pipeline of anticancer drugs.

Molecular Therapy—Nucleic Acids (2014) **3**, e159; doi:10.1038/mtna.2014.9; published online 29 April 2014
Subject Category: siRNAs, shRNAs, and miRNAs Therapeutic proof-of-concept

Introduction

Selective downregulation of gene expression by small interfering RNA (siRNA) provides a powerful approach for treating a wide range of human diseases, including cancers.[1,2] Indeed, several studies have demonstrated the potential of siRNA-based therapeutics for inhibiting the growth and proliferation of cancer cells both *in vitro* and *in vivo*.[3–5] Furthermore, siRNA-based therapeutics have shown considerable potential in sensitizing cancer cells to chemotherapy by silencing genes that contribute to the drug resistance that can occur during chemotherapy.[6,7]

In this study, we took an RNA interference (RNAi) approach to target the mitochondrial protein voltage-dependent anion channel 1 (VDAC1), a key protein in cell metabolism. Lying in the outer mitochondrial membrane (OMM), VDAC1, also known as mitochondrial porin, assumes a crucial position in the cell, forming the main interface between the mitochondrial and cellular metabolisms.[8] Permeable to molecules up to ~5,000 Da, VDAC1 mediates the flux of ions, nucleotides, and other metabolites across the OMM. VDAC1 thus enables substrates, including pyruvate, malate, succinate, and NADH, to enter the mitochondria and mediates the exit of newly formed molecules, such as hemes, from the mitochondria.[8] VDAC1 is also involved in the mitochondrial entry and exit of Ca^{2+}[9,10] endoplasmic reticulum-mitochondria crosstalk[11–13] and functions in cholesterol transport across the OMM.[14] Specifically, VDAC1 has been proposed to be a necessary component of a protein complex involved in mitochondrial membrane cholesterol distribution and transport and to play an important role in altered cholesterol synthesis and transport in Morris hepatoma cells.[15] In this respect, it has been recently shown that effective cholesterol efflux is critical for proper angiogenesis.[16]

In addition to the multifunctional role of VDAC1 in energy production and metabolism, the location of VDAC1 at the boundary between the mitochondria and the cytosol allows for its interaction with proteins that mediate and regulate the integration of mitochondrial functions with other cellular activities. VDAC1 interacts with hexokinase and creatine kinase to convert newly generated adenoside triphosphate (ATP) into high-energy storage molecules, such as glucose-6-phosphate (G-6-P) in the brain and creatine phosphate in muscle.[17] These findings portray VDAC1 as a dynamic regulator of global mitochondrial functions in both health and disease.[18,19] As such, the overexpression of VDAC1 observed in several cancer types may be related to those activities of the protein required by highly metabolically active and energy-demanding cancer cells.[20]

Given the ability of VDAC1 to mediate the traffic of nutrients and metabolites across the OMM, thereby controlling cell energy and metabolic homeostasis, downregulation of VDAC1 expression should result in decreased cell energy

The first two authors contributed equally to this work.
[1]Department of Life Sciences and, The National Institute for Biotechnology in the Negev, Ben-Gurion University of the Negev, Beer-Sheva, Israel; [2]Department of Cardio-Thoracic Surgery, Soroka University Medical Center and the Faculty of Health Sciences, Ben-Gurion University of the Negev, Beer-Sheva, Israel. Correspondence: Varda Shoshan-Barmatz, Department of Life Sciences, The National Institute for Biotechnology in the Negev, Ben-Gurion University of the Negev, Beer-Sheva 84105, Israel. E-mail: vardasb@bgu.ac.il
Keywords: cancer; mitochondria; small interfering RNA; voltage-dependent anion channel 1
Received 29 October 2013; accepted 16 February 2014; published online 29 April 2014. doi:10.1038/mtna.2014.9

production and growth. Accordingly, we have previously demonstrated that short hairpin VDAC1 RNA (shRNA-VDAC1) specifically silenced VDAC1 protein expression and disrupted energy production and cell growth[21] and inhibited tumor development in animal models.[22] In the current study, synthetic siRNA directed to a sequence specific for human VDAC1 was shown to silence VDAC1 expression, to decrease cellular ATP levels, and to inhibit cell growth and migration, and when injected into established tumors in a xenograft lung cancer mouse model, it not only inhibited tumor growth but also led to tumor regression.

Results

As VDAC1 functions in cell energy and metabolism, interfering with such activities in cancer cells via siRNA-mediated silencing of VDAC1 expression should affect the growth of these high energy-demanding cells. Accordingly, the requirement for VDAC1 in cancer cell growth was addressed by silencing VDAC1 expression by means of siRNA. In addition, the antitumor activity of VDAC1-based siRNA in mouse models of lung cancer was demonstrated.

VDAC1-specific silencing by siRNA

VDAC1 silencing by hVDAC1-siRNA was tested in several human-derived cancer cell lines of various origin. These included A549 and H358 non-small lung carcinoma cells, PC3 prostate cancer cells, U-87 human glioblastoma cells, Panc-1 pancreas cancer cells, HCT116 human colon carcinoma cells, Hep2G human hepatocellular carcinoma cells, and noncancerous human embryonic kidney (HEK)-293 human embryonic kidney (**Figure 1**), HaCat, and pancreatic

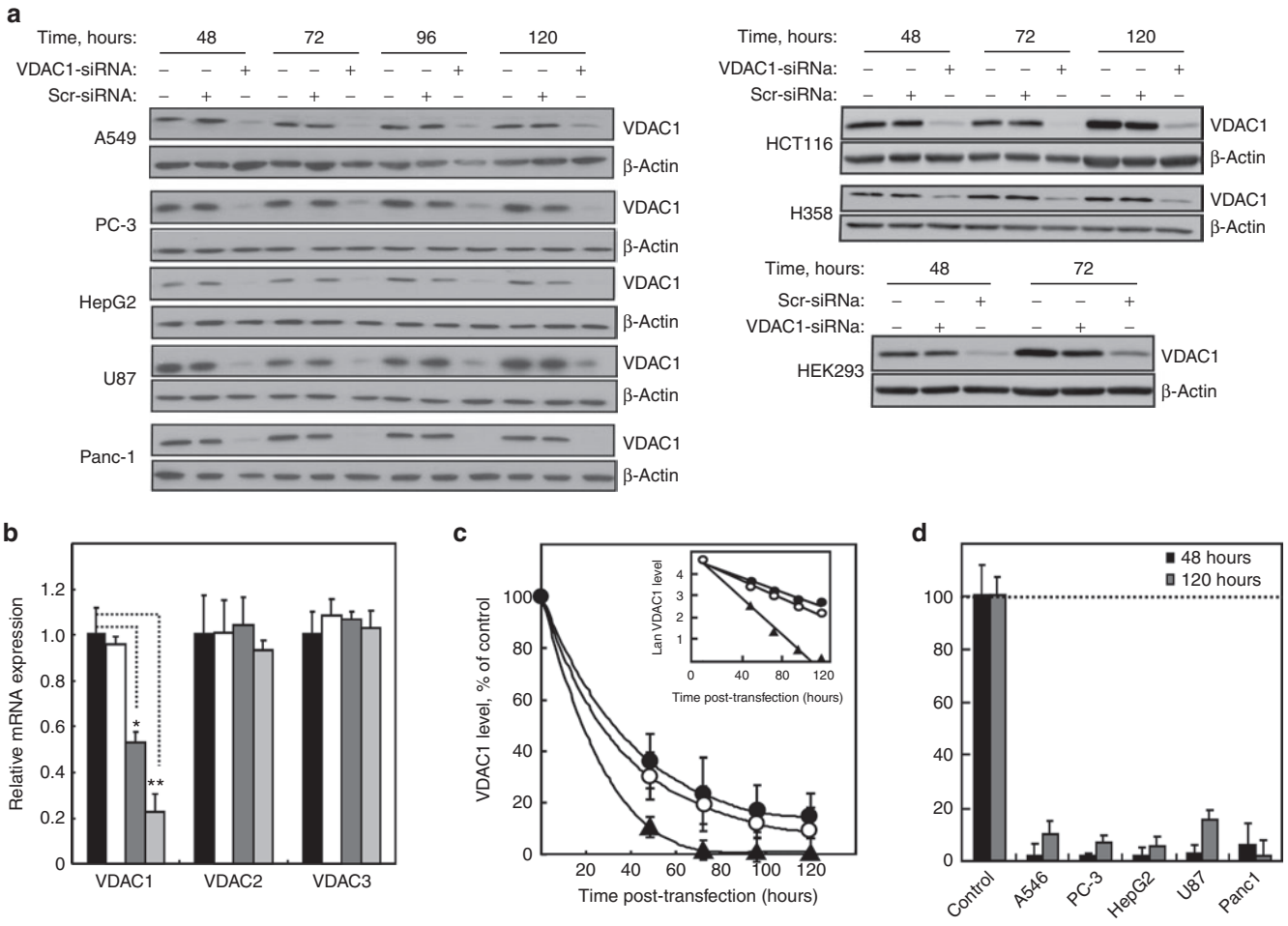

Figure 1 hVDAC1-siRNA-silenced VDAC1 expression in various cancer cell lines. In (**a**), several cancer cell lines were either not transfected (control) or transfected with scrambled (Scr-siRNA) or VDAC1-specific siRNA (VDAC1-siRNA) and analyzed for VDAC1 expression at the indicated times post-transfection using anti-VDAC1 antibodies. Cells transfection was carried out using 50 nmol/l siRNA and the following transfection reagents: HCT116 and HEK-293 cells were transfected using DharmaFect, H358 and A549 cells and PC-3, Panc-1, U-87, and HeLa cells were transfecting using Jet Prime, while HepG2 cells were transfected using INTERFERin. In (**b**), qPCR analysis of mRNA isolated from A549 cells not treated (black bars) or treated with 50 nmol/l scrambled-siRNA (white bars) or with VDAC1-siRNA, 25 nmol/l (dark gray bars) or 50 nmol/l (light gray bars). VDAC1, VDAC2, and VDAC3 levels were analyzed using specific primers and probes as described in Materials and Methods. In (**c**), Densitometric quantitative analysis of the immunoblot was carried out and presented (relative units (RU)) for all cell lines 48 and 120 hours post-transfection ($n = 3$). In (**d**), showing that VDAC1 expression levels were reduced by about 90%. This decrease persisted for up to 120 hours post-transfection. The decreases in voltage-dependent anion channel (VDAC) levels as function of time post-transfection for three cell lines ($n = 3$), with the inset showing analysis of half-life time ($t_{1/2}$) of VDAC1-silencing, are presented.

MIN-6 cell lines (**Figure 4**). VDAC1 levels following siRNA silencing were analyzed by immunoblotting using anti-VDAC1 antibodies. Such analysis revealed that the hVDAC1-siRNA used effectively silenced VDAC1 expression by about 90% in all tested cell lines at relatively low concentration (50 nmol/l), using the appropriate transfection reagent (**Figure 1**).

Moreover, the hVDAC1-siRNA used specifically decreased the level of VDAC1 mRNA but had no effect on that of VDAC2 or VDAC3 (**Figure 1b**). The decrease in VDAC1 mRNA was concentration-dependent, decreasing by 50 and 75% when cells treated with 25 and 50 nmol/l siRNA respectively, values in agreement with the decreases in protein expression levels seen. These results clearly indicate the specificity of the siRNA used toward VDAC1.

The overall decrease in the level of VDAC1 was about 90% in all cell lines examined, with this low level of the protein being maintained from 36 up to 144 hours post-transfection (**Figure 1c**). Indeed, a relatively rapid decrease in VDAC1 levels was observed following silencing of its expression, with the decrease reaching 50% ($T_{1/2}$) in about 34 and 39 hours for A549 and U87 cells, respectively and 16 hours for Panc cells (**Figure 1d**).

The decrease in VDAC1 expression was constant up to about 144 hours following a single transfection. Thereafter, the protein expression level was gradually restored with time, recovering from the 90% decrease seen after 144 hours to 35% decrease 196 hours post-transfection (**Figure 2A–B**). Such a decrease in VDAC1 silencing is expected due to siRNA degradation and dilution as a result of some degree of cell division. However, VDAC1 silencing could be extended up to 240 hours (10 days) by a second transfection with VDAC1-siRNA on day 5 following the first transfection (**Figure 2C,c**).

The sequence of VDAC1 is greatly conserved between humans and mice, differing by only 3 of the 282 amino acids comprising the protein.[8] As such, the 21 bp human VDAC1-siRNA used in this study was designed with a nucleotide sequence (238–256) corresponding to a region of human VDAC1 (hVDAC1), which differs from the murine sequence by four nucleotides (**Figure 2D**). To demonstrate the specificity of VDAC1-siRNA for human VDAC1, human HCT116 colon cancer cells and murine CT26 colon cancer cells were both transfected with hVDAC1-siRNA, and VDAC1 expression levels were analyzed by western blot. The results show that hVDAC1-siRNA prevented VDAC1 expression in the cells of human origin but had no effect on VDAC1 expression in the murine cells (**Figure 2E**). This allowed the use of hVDAC1-siRNA in mice carrying human-derived cancer cells.

VDAC1 silencing results in a dramatic inhibition of cell proliferation

As VDAC1 levels pose a limit to nutrient and metabolite traffic across the OMM, VDAC1 downregulation by siRNA should affect cancer cell growth. VDAC1 silencing resulted in a dramatic decrease in cell growth of all cell lines tested, namely A549, PC3, HepG2, U-87, HeLa, and Panc-1 cells (**Figure 3a–f**), as well as HCT116 and H358 cells (data not shown), as analyzed by the sulforhodamine B (SRB) assay. The 80–90% decrease in cell proliferation was constant for up to 144 hours post-transfection with VDAC1-siRNA, as

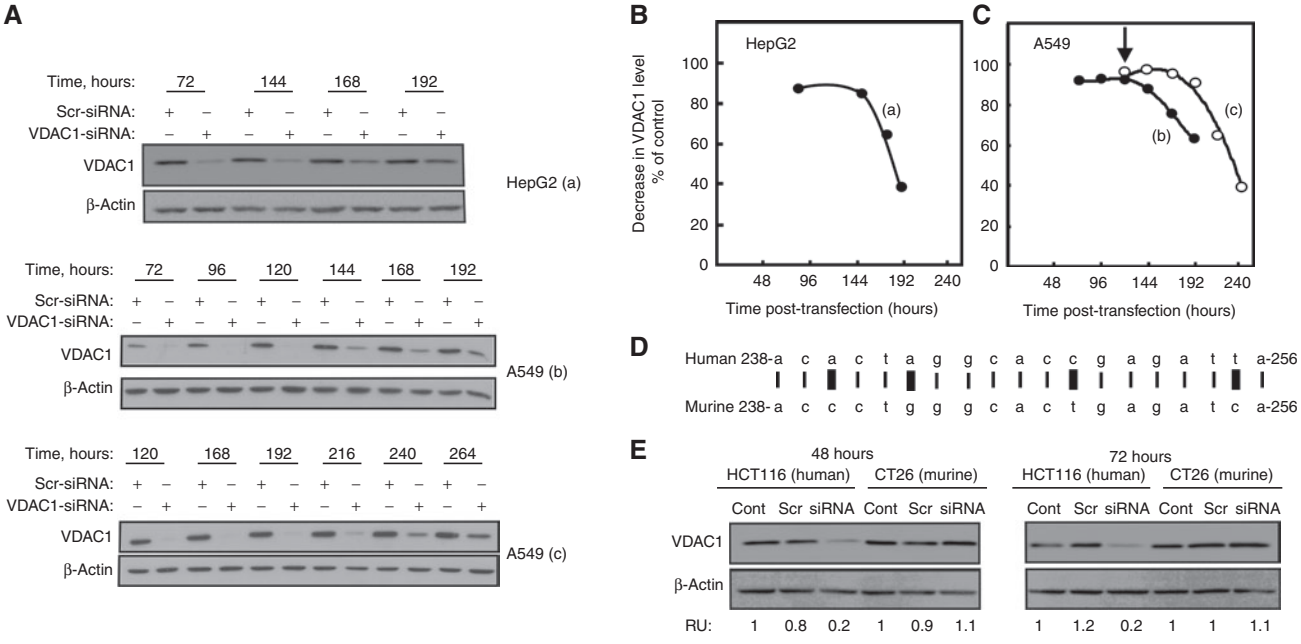

Figure 2 Time course of small interfering RNA (siRNA)-silencing of voltage-dependent anion channel (VDAC1) expression and its specificity for human VDAC1. (**A**) HepG2 (**a**) and A549 (**b, c**) cells were transfected with scrambled (Scr) or VDAC1-siRNA (siRNA) (50 nmol/l), and VDAC1 levels were analyzed at the indicated times. Quantitative analysis representing the decrease in VDAC1 levels as a function of the time post-transfection in HepG2 (**b**) and A549 (**c**) cells is presented. In **C**, cells were divided into two groups 120 hours post-transfection (**b** and **c**), with cells in (**c**) being subjected to a second transfection with VDAC1-siRNA (50 nmol/l). VDAC1 levels were analyzed in each case. Quantitation of the results is presented in **C**. In **D**, sequences of the human and murine VDAC1 siRNA, differing by four nucleotides (indicated by rectangles), are shown. In **E**, human HCT-116 and murine CT26 colon carcinoma cells were transfected with hVDAC1-siRNA and VDAC1 expression was analyzed 48 and 72 hours post-transfection. Quantitative densitometric analysis is presented as relative units (RU).

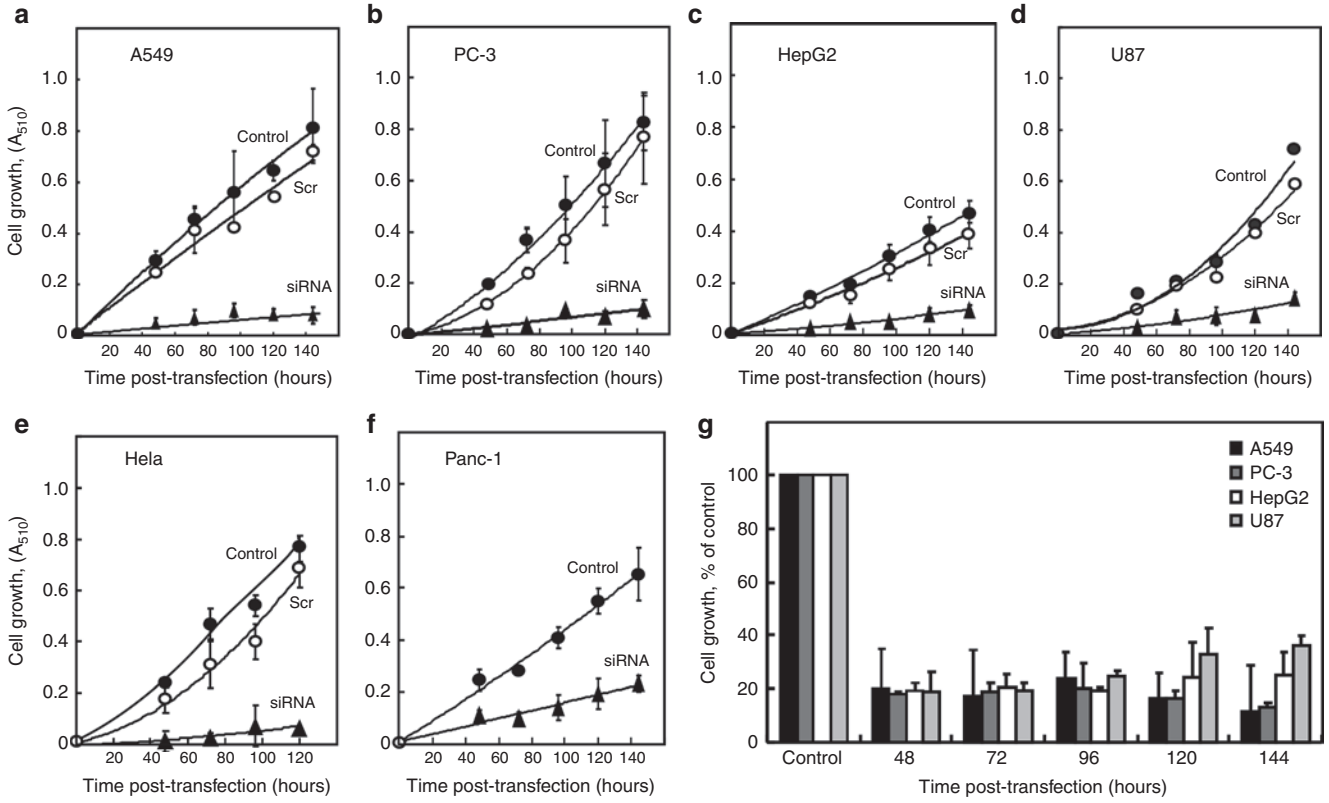

Figure 3 Effect of voltage-dependent anion channel (VDAC1)-silencing on cell growth. Cell growth of the A549 (**a**), PC-3 (**b**), HepG2 (**c**), U-87 (**d**), HeLa (**e**), and Panc-1 (**f**) cell lines was assayed using the sulforhodamine B (SRB) cell proliferation assay, presented as absorbance at 510 nm. Cells were nontransfected (control) (•) or transfected with scrambled (Scr) (o) or VDAC1-siRNA (siRNA) (▲) (50 nmol/l), and cell amounts were analyzed at the indicated times (48–144 hours) post-transfection. Cell growth at 48, 72, 96, 120, and 144 hours post-transfection with VDAC1-siRNA is presented as a percent of the cell growth attained by scrambled small interfering RNA (siRNA)-transfected cells (**g**) ($n = 3$).

compared to cells transfected with scrambled siRNA which had no significant effect on cell growth (**Figure 3g**).

As the amount of protein is analyzed by the SRB-based method, the decrease in VDAC1 levels obtained upon VDAC1-siRNA treatment could reflect a decrease in the number or size of the transfected cells. Therefore, a colony-forming assay was performed (**Figure 4a**). A549 cells were transfected with scrambled- or VDAC1-siRNA, and 24 hours later, equal numbers of cells were seeded. Proliferating colonies were scored 96 hours post-transfection, and the number of colonies in VDAC1-siRNA–transfected cells was found to be reduced by 86% for A549 cells (**Figure 4a**, right panel), in correlation with the degree of VDAC1 silencing seen, *i.e.*, 90%, (**Figure 4a**, left panel).

To verify whether VDAC1 silencing also led to cell death, apoptosis was analyzed by Annexin V and propidium iodine staining followed by flow cytometric analysis. Control cells or cells transfected with scrambled- or VDAC1-siRNA showed similar low (5–8%) degrees of cell death (data not shown). These results indicated that the decrease in cell growth seen upon silencing VDAC1 expression is due to inhibition of cell proliferation and not enhanced cell death.

Next, we compared the effects of VDAC1 silencing on the growth of cancer cell line A549 and noncancer immortal human keratinocyte HaCaT and pancreatic (MIN-6) cell lines as a function of siRNA concentration (5–50 nmol/l) (**Figure 4b–d**). At very low concentrations (5–10 nmol/l), VDAC1-siRNA similarly silenced the expression of VDAC1 in the three cell types by about 90% (**Figure 4b**). In contrast, VDAC1-siRNA inhibited A549 cell growth, as assayed by both cells total protein determination, sulforhodamine B assay (SRB) (**Figure 4d**) and cell survival assay, XTT (**Figure 4c**) methods, while inhibiting the growth of HaCaT and MIN-6 cells to a lesser extent when applied at higher concentrations. These results point to the specificity of VDAC1-siRNA toward cancer cells. This effect could result from the requirement of cancer cells for VDAC1-related functions, as reflected in the overexpression of VDAC1 in various cancer cell lines by up to about fourfold, relative to VDAC1 levels in the noncancerous transformed cells (HEK) (**Figure 4e**).

The overexpression of VDAC1 in cancer cells was further demonstrated by comparing VDAC1 levels in lung tissue samples taken from healthy and tumor areas of the same patient (**Figure 4f**). The results clearly demonstrated that in all tissue samples collected from 11 patients, VDAC1 is overexpressed in the tumor tissue at levels up to over eightfold higher than in the healthy tissue.

VDAC1 silencing results in decreased mitochondrial membrane potential, cellular ATP levels and affects reactive oxygen species production

As VDAC1 controls the metabolic crosstalk between the cytosol and mitochondria, we tested the effect of VDAC1 silencing on the metabolic activity of mitochondria, including membrane potential ($\Delta\Psi$), cellular ATP levels and production of reactive

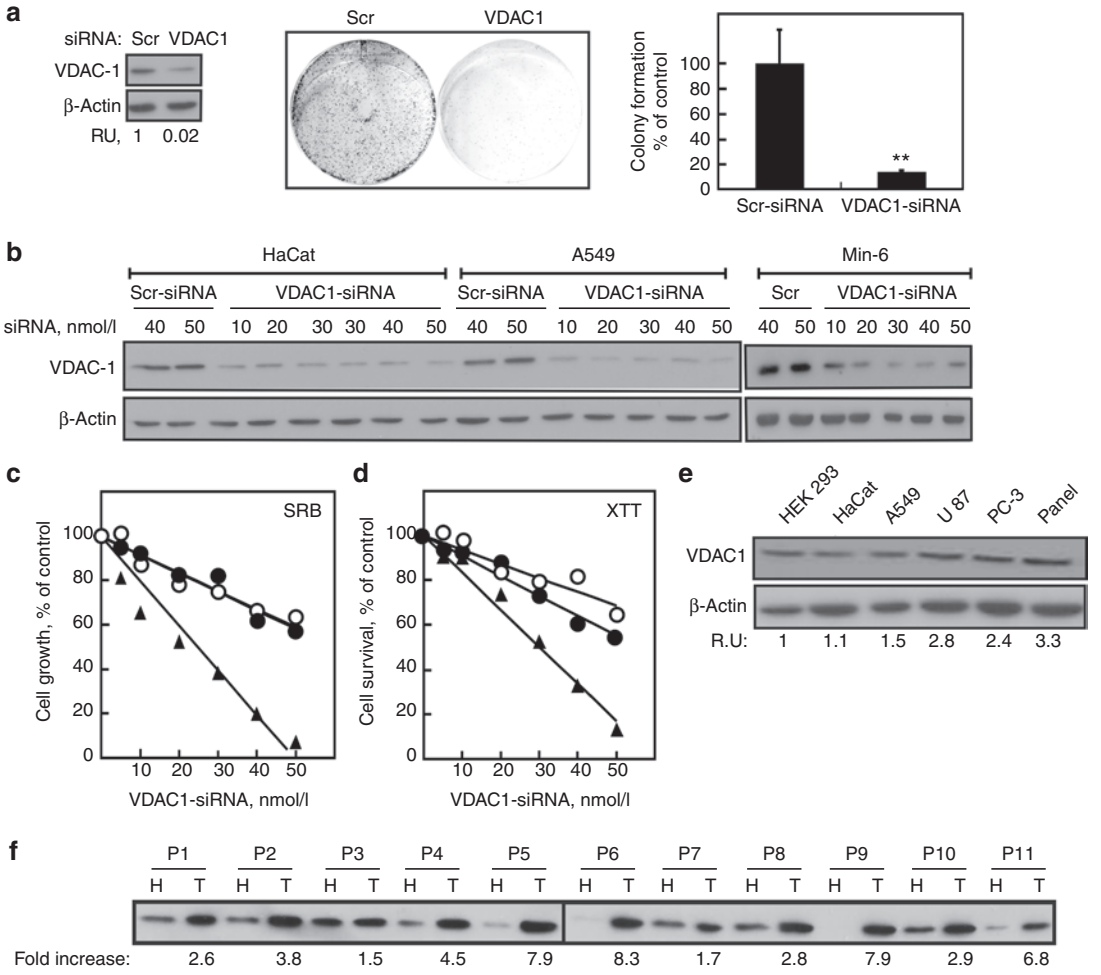

Figure 4 Cell proliferation and growth of cancer cells expressing highly levels of voltage-dependent anion channel (VDAC1) are highly inhibited by VDAC1-siRNA. A549 (**a**) cells were transfected with scrambled (Scr) or hVDAC1-small interfering RNA (siRNA) (VDAC1) and were analyzed for VDAC1 expression levels 96 hours post-transfection (**a**, left panel). The relative amount (RU) of VDAC1 in the treated cells, in comparison to controls, is presented. Colony formation analysis of controls and VDAC1-silenced cells (**a**, center panel) was carried out as described in Material and Methods. Quantitative analysis of colonies (**a**, right panel) is presented as means ± SEM (**$P < 0.01$; $n = 3$). In **b**, A549 and immortal human keratinocyte HaCat and pancreatic (MIN-6) cell lines were transfected with scrambled or VDAC1-siRNA, and 48 hours post-transfection, the cell lines were analyzed for VDAC1 expression levels by immunblot (**b**), and cell growth of A549 (▲), HaCat (O) and Min-6 (•)using sulforhodamine B (**c**) or XTT (**d**). In **e**, the levels of VDAC1 in several cancer cell lines, relative to such levels in noncancerous HEK cells, are presented. In **f**, samples of healthy (H) and tumor (T) tissues, each taken from the same lung of a lung cancer patient, were obtained and prepared for sodium dodecyl sulfate–polyacrylamide gel electrophoresis (SDS–PAGE) and immunoblot, as described in the Materials and Methods section. The fold increase in VDAC1 expression represents the increase in VDAC1 level in the tumor in comparison to the healthy tissue, both from the same patient. As actin levels differed in healthy and tumor tissues, we did not use actin as a loading control. However, the same protein amounts were loaded, as evaluated by protein determination using the Lowery method and by SDS–PAGE, Commassie blue staining and quantitative analysis of proteins band intensity.

oxygen species (ROS). $\Delta\Psi$ was tested using tetramethylrhodamine methylester (TMRM) as a cationic mitochondria-selective probe and by cytofluorometric analysis. A549, PC3, and HePG3 cells treated with hVDAC1-siRNA showed a decrease of about 40% in $\Delta\Psi$, as compared to controls (**Figure 5a**). As expected from the decrease in $\Delta\Psi$ observed in cells with low VDAC1 levels, cellular ATP levels were also decreased by about 50% in such cells (**Figure 5b**), suggesting that mitochondrial energy production is affected by the absence of VDAC1.

As mitochondria with limited metabolites might act inefficiently, leading to ROS production, ROS levels in the cytosol and mitochondria were assessed using DCFDA and MitoSOX, respectively. Cell transfected with hVDAC1-siRNA showed about 2.6- and 6.9-fold increases in cytosolic and mitochondrial ROS levels, respectively. These increased levels are, however, 11-fold less than the degree of cytosolic ROS produced by As_2O_3 or the level of mitochondrial ROS produced by rotenone (**Figure 5c–e**). The higher increase in mitochondrial ROS in comparison to what is seen in the cytosol of VDAC1-depleted cells is expected, as ROS crosses the OMM via VDAC1.[23]

VDAC1 siRNA-treated cells show lower cell motility

Next, we tested the effect of silencing VDAC1 expression on cell migration in A549 cells (**Figure 6**) using a wound-healing assay.[24] A fixed-width scratch was created in a cell monolayer 72 hours post-transfection with scrambled- or VDAC1-siRNA,

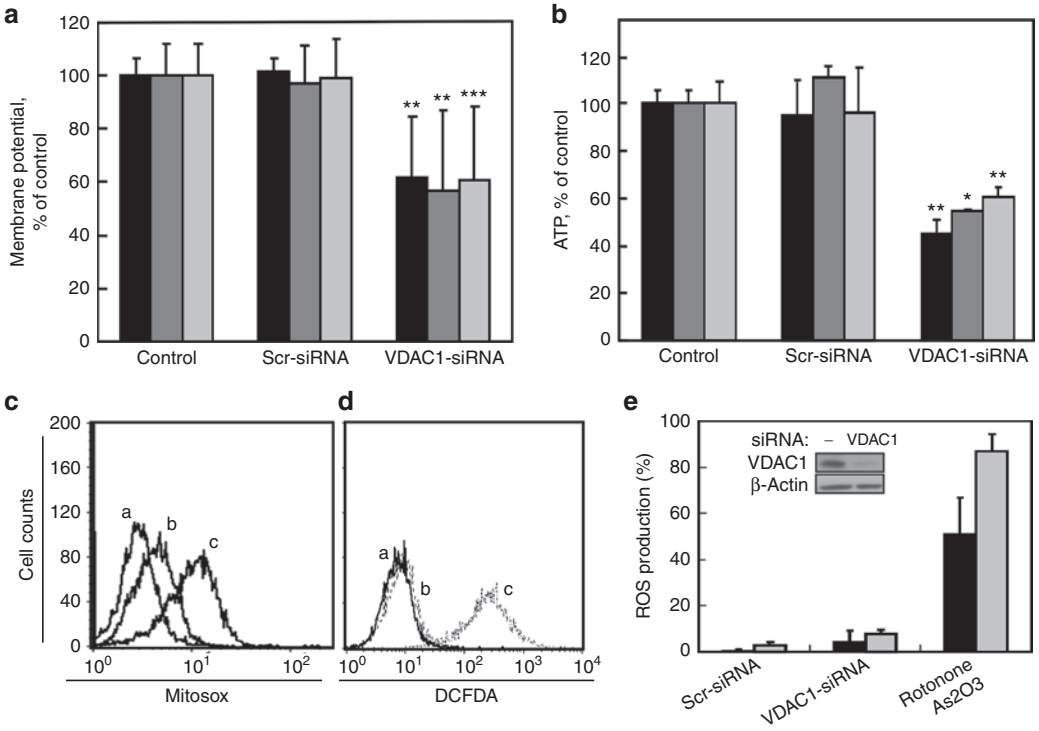

Figure 5 Decreased mitochondrial membrane potential and cellular ATP levels in cells silenced for voltage-dependent anion channel (VDAC1) expression. HepG2 (black bars), A549 (dark grey), and PC-3 (grey) cells were untreated (control) or treated with scrambled or VDAC1-small interfering RNA (siRNA) and analyzed for mitochondrial $\Delta\Psi$ with tetramethylrhodamine methylester (TMRM) (**a**), or for ATP cellular levels HepG2 (black bars), A549 (dark gray), and PC-3 (gray) (**b**), as described in Materials and Methods. Values represent means ± SEM ($n = 3$). Mitochondrial and cytosolic reactive oxygen species levels in A549 cells treated with scrambled- or VDAC1-siRNA were analyzed (**c, d**) as described in the Materials and Method section. To validate the assays, control cells were also treated with rotenone (10 µm, 16 hours) or As_2O_3 (80 µm, 16 hours). The results of fluorescence-activated cell sorting analysis (a representative experiment is shown in **c** and **d**) with mean ± SEM ($n = 3$) are presented (**e**), as well as the VDAC1 level in scrambled- and VDAC1-siRNA-treated cell is presented (inset, **e**).

and the progress of the migrating front was monitored using a digital camera coupled with a microscope. In comparison to cells transfected with scrambled siRNA, cells silenced for VDAC1 expression by about 90% (**Figure 6c**) showed decreased migration in both the absence and presence of basic fibroblast growth factor (bFGF), known to accelerate wound healing.[25] In the presence of bFGF, control cells migrated significantly faster toward the gap than in the absence of the factor. VDAC1-depleted cells showed attenuated migration that was further pronounced upon bFGF treatment, with VDAC1-siRNA-treated cell migrating six-fold slower (**Figure 6a**,**b**). The decrease in cell migration in VDAC1 expression-silenced cells was not due to a decrease in cell proliferation ability, as decreased cell migration was observed even after 6 hours in hVDAC1-siRNA-treated cells showing no significant difference in cell numbers (data not shown).

hVDAC1-siRNA inhibits proliferation of HepG2 cells in Matrigel plugs implanted in nude mice

To demonstrate the effect of hVDAC1-siRNA *in vivo,* we used the Matrigel plug implant method (**Figure 7**). HepG2 cells transfected with hVDAC1-siRNA and control nontransfected cells were stained with the Vybrant DiD cell-labeling reagent and subsequently mixed with liquid Matrigel at 4 °C. The cells-Matrigel mixture was injected subcutaneously (s.c.) into the interscapular region of nude mice, leading to the formation of plugs in this 37 °C environment. The mice were exposed to bromodeoxyuridine (BrdU) in the drinking water to label proliferating cells in both mouse tissues and the implanted human HepG2 cell population. After 7 days, the mice were sacrificed and the implanted cells were extracted from the plugs by enzymatic digestion and analyzed by fluorescence activated cell sorting (FACS) to distinguish between cancer cells labeled with both DiD and BrdU and mouse cells labeled with BrdU alone. A substantial decrease in cell growth (65%) of hVDAC1-siRNA-treated cells as compared with nontransfected control cells (**Figure 7b**) was seen. It should be noted that under the conditions employed, VDAC1 expression levels in the plug-implemented siRNA-treated cells was also decreased by 65–75% (**Figure 7a**). These results suggest that hVDAC1-siRNA suppressed cell proliferation *in vivo*.

hVDAC1 siRNA inhibits tumor growth in nude mice

Next, we tested whether hVDAC1-siRNA could affect an established lung tumor using a xenograft nude mice model. For this experiment, we used a more stable siRNA, which was selected from a set of 2′-O-Me-modified hVDAC1-siRNAs. Three different combinations of modifications (comprising 5–7 methylations) of hVDAC1-siRNA (si-hVDAC1 1/A, si-hVDAC1 2/A, and si-hVDAC1 2/B) were designed and tested for their VDAC1-silencing activities (**Figure 7c**–**e**).

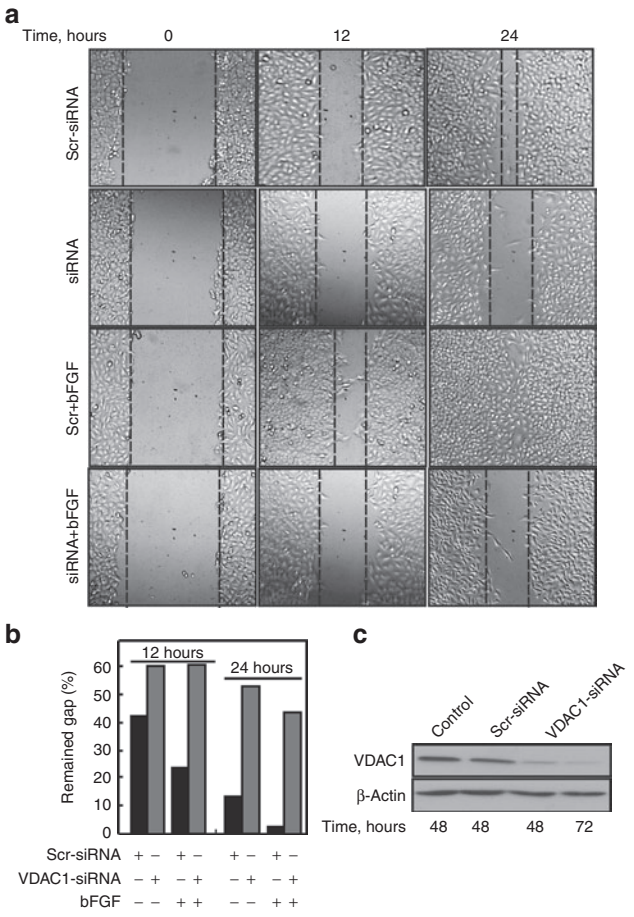

Figure 6 The effect of voltage-dependent anion channel (VDAC1) deletion on cancer cell migration. A549 (**a**) cells were treated with scrambled or VDAC1-small interfering RNA (siRNA) and allowed to grow to 80% confluency (72 hours). The semiconfluent cell layer was scraped using a 200-µl sterile pipette tip to create a scratch/wound devoid of cells. Where indicated, cells were treated with basic fibroblast growth factor (20 µg/ml). Migration was assessed at 12 and 24 hours after treatment (60 and 72 hours post-transfection), as evaluated by the wound-healing assay. Representative photomicrographs are shown. (**b**) Quantification of the results describes the change in percentage of the scratch size at the indicated times. Data shown represent means ± SEM (n =3). $^{**}P < 0.01$, treated versus control. (**c**) The level of VDAC1 in control cells and in cells transfected with scrambled or VDAC1-siRNA is presented.

Treatment with hVDAC1-siRNA 2/A and nonmodified hVDAC1-siRNA led to similar VDAC1 silencing effects (>90%) in both HepG2 (data not shown) and A549 cells (**Figure 7c**,**d**). The modified si-hVDAC1 1/A and si-hVDAC1 2/B sequences were less effective, decreasing expression by about 70 and 80%, respectively. As expected, scrambled siRNA had no effect on VDAC1 levels (**Figure 7c**,**d**). Moreover, hVDAC1-siRNA 2/A inhibited the growth of A547 cells by about 90%, with such inhibition lasting up to 144 hours post-transfection (**Figure 7e**).

Following validation of A549 cell growth inhibition upon transfection with modified hVDAC1-siRNA, we tested the effects of such treatment on tumor growth *in vivo* (**Figure 8**). Nude mice were injected s.c. with A549 lung cancer cells and allowed 11 days for tumor formation (65–110 mm^3). The mice were then split into three matched groups, with groups being injected every 3 days with phosphate-buffered saline (PBS) (group 1), scrambled siRNA (group 2), or hVDAC1-siRNA2/A (group 3). Tumor growth was then followed for about 23 days. The results show tumor growth in both PBS- and scrambled siRNA-injected tumors, where the tumor volume grew exponentially as expected and increased over 3.5-fold in size in 20 days (**Figure 8a**). On the other hand, the tumors in hVDAC1-siRNA2/A-injected mice not only did not grow further but shrank in volume to levels 60% lower than the original volume measured before VDAC1-siRNA injection (**Figure 8a**). Comparing tumor sizes at the end point revealed the average tumor volume in control- and scrambled siRNA-injected animals to be about 8- to 10-fold larger than that in the hVDAC1-siRNA2/A-treated mice. The differences in tumor volume between the control groups (groups 1 and 2) and the hVDAC1-siRNA2/A-treated mice at all-time points were highly significant ($P < 0.001$). The general health of the mice, as monitored by following their weight, was found to change similarly in the three treatment groups.

Statistical analysis of these results using repeated measures analysis of variance to evaluate tumor growth rate starting from the day of injection onward indicated that changes in tumor volume over time were not consistent across the three treatment groups. These relative growth rates translated into daily increases of 5.38 and 4.38% in the tumor volume of mice in the PBS- and scrambled siRNA-treated groups, respectively. In contrast, tumor volume in mice from the VDAC1-siRNA-treated group decreased by 2.77% per day. This further demonstrated the effect of VDAC1-siRNA not only in inhibiting tumor growth but also in reducing the size of the original tumor (**Figure 8b**). Finally, the mice were sacrificed 23 days after injection, the tumors were excised (**Figure 8c**), and their weights were determined (**Figure 8d**). The results obtained were similar to those based on the calculated tumor volumes (**Figure 8a**).

VDAC1 expression levels were also analyzed in lysates prepared from tumors from the three treated groups using anti-VDAC1 antibodies recognizing both human and mouse VDAC1. VDAC1 levels in the tumors from si-hVDAC1 2/A-treated mice were lower than in the PBS- and scrambled siRNA-injected tumors (**Figure 8e**).

Finally, histological analysis of paraffin sections cut from tumors removed from PBS-, scrambled-, and VDAC1-siRNA-treated mice was carried out by hematoxylin/eosin and immunohistochemical staining with anti-VDAC1 antibodies, recognizing both mouse and human proteins (**Figure 8f**). Representative sections from each group revealed similar staining in PBS- and scrambled siRNA-injected tumors, with homogenous and strong staining being seen with anti-VDAC1 antibodies. The sections from the hVDAC1-siRNA2/A–injected tumor showed nonhomogenous staining, with strong staining representing a tumor containing A549 lung cancer cells, while some nonstained areas most likely represent cells of mouse origin (**Figure 8f**, arrow heads).

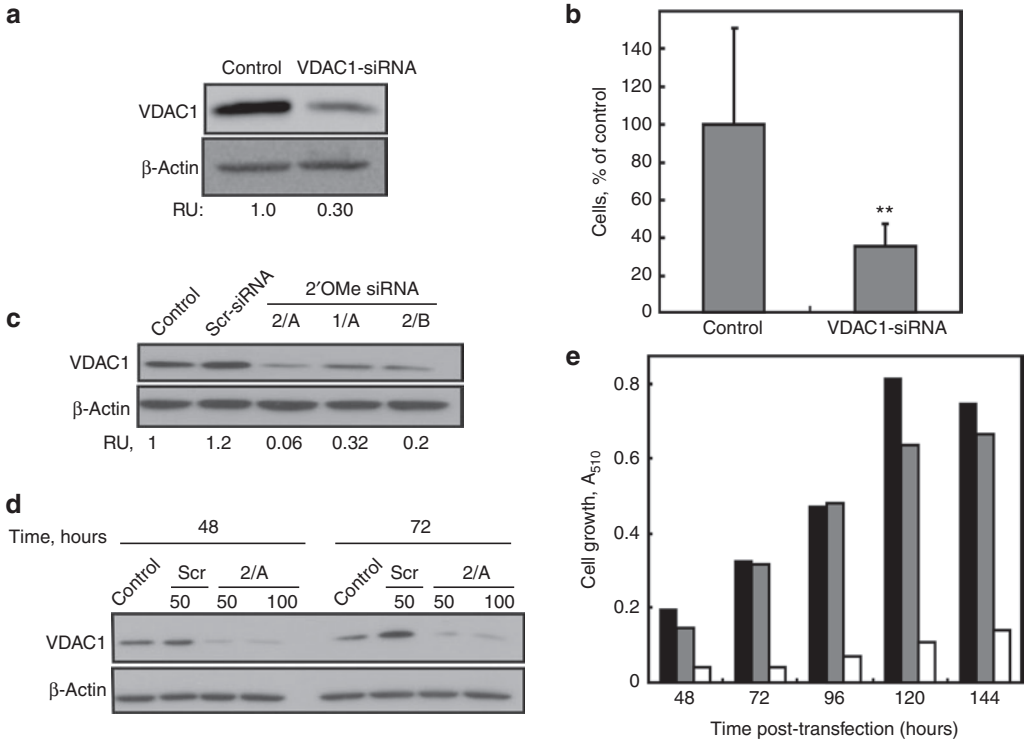

Figure 7 Unmodified and modified hVDAC1-siRNA inhibition of cell growth *in vitro* and *in vivo* in Matrigel plug implants placed in nude mice. HepG2 cells were untreated or transfected with hVDAC1-siRNA (50 nmol/l) and their growth was tested *in vivo* using the Matrigel plug assay. DiD-labeled cells were inoculated into nude mice s.c., which were then provided with bromodeoxyuridine-containing water. After 5 days, the plugs were removed and sequentially analyzed for (**a**) voltage-dependent anion channel (VDAC1) expression levels and (**b**) cell proliferation. Cell growth was reduced by 65% in VDAC1-siRNA-transfected cells ($n = 12$), as compared to control cells ($n = 9$). The results represent means ± SEM, $^{**}P < 0.01$ for hVDAC1-siRNA-transfected cells, as compared with control mice. In **c**, A549 cells were transfected with 50 nmol/l modified 1/A-, 2/A-, and 2/B-siRNA-hVDAC1 or scrambled small interfering RNA (siRNA). Fourty-eight hours post-transfection, the cells were harvested, lysed, and VDAC1 expression level was evaluated by immunoblot. Densitometric quantification analysis is presented as relative units (RU). A549 cells were untransfected or transfected with scrambled or 2/A-VDAC1-siRNA (50 or 100 nmol/l) and VDAC1 expression levels (**d**) and cell growth, assayed using (**e**) the sulforhodamine B (SRB) method, were assessed 48 and 72 hours or 96, 120, and 144 hours post-transfection, respectively. Black, grey, and white bars represent untransfected, transfected with scrambled or hVDAC1-siRNA cells, respectively ($n = 2$).

Discussion

RNAi-based therapies present several advantages over more conventional therapeutic approaches, given the highly selective silencing of target protein expression and the limited toxic side effects.[1] siRNA molecules thus offer a promising approach for the development of a powerful class of gene expression–specific inhibitors that can be used to combat cancer and other diseases.[26] Indeed, several *in vivo* studies using animal models have already demonstrated that RNAi-based therapeutics are effective for the treatment of various diseases, such as viral hepatitis,[27] Huntington's disease,[28] and some cancers.[29] Here, we demonstrated the potential of silencing VDAC1 expression in cancer cells by specific siRNA as an anticancer therapeutic agent, inhibiting tumor growth and inducing regression of existing tumors. VDAC1 is highly expressed in different cancer cell lines and tumors (**Figure 4f**,**g**),[19,30] suggesting that this protein contributes to the highly active metabolism of cancer cells. Thus, depletion of VDAC1 would be expected to predominantly affect such cells.[31] In fact, previous *in vivo* studies from our laboratory using HeLa cancer cells expressing VDAC1-shRNA from an inducible promoter and injected into nude mice showed inhibition of solid tumor development.[22]

Human-specific VDAC1-siRNA effectively silences VDAC1 expression and inhibits cell growth and migration by hindering VDAC1 function in cell energy and metabolism

Our results demonstrate that at relatively low concentrations (5–50 nmol/l), human-specific siRNA silenced the expression of VDAC1 by 80–90% in different human cancer cell lines (**Figures 1**, **2** and **7**). Moreover, the siRNA used in the current study is specific to VDAC1 and had no effect on VDAC2 and VDAC3 mRNA levels, as demonstrated using quantitative polymerase chain reaction (qPCR) (**Figure 1b**). While such VDAC1 silencing occurs rapidly and lasts for over a week, it can be extended for up to 2 weeks upon a second transfection (**Figure 2**). The 6-day interval for transient transfection could potentially allow therapeutic applications, whereby the siRNA would be administered once a week. Because VDAC1 silencing by siRNA induced growth inhibition by over 85% in all nine cancer cell lines tested but only slightly affected the growth of noncancerous cells *in vitro* (**Figure 4c**), it is reasonable to assume that such treatments will be effective in other cancer cells of human origin. Furthermore, VDAC1 silencing resulted not only in inhibition of cell growth but also in cell eradication, as reflected by the results of the colony assay employed here (**Figure 4a**).

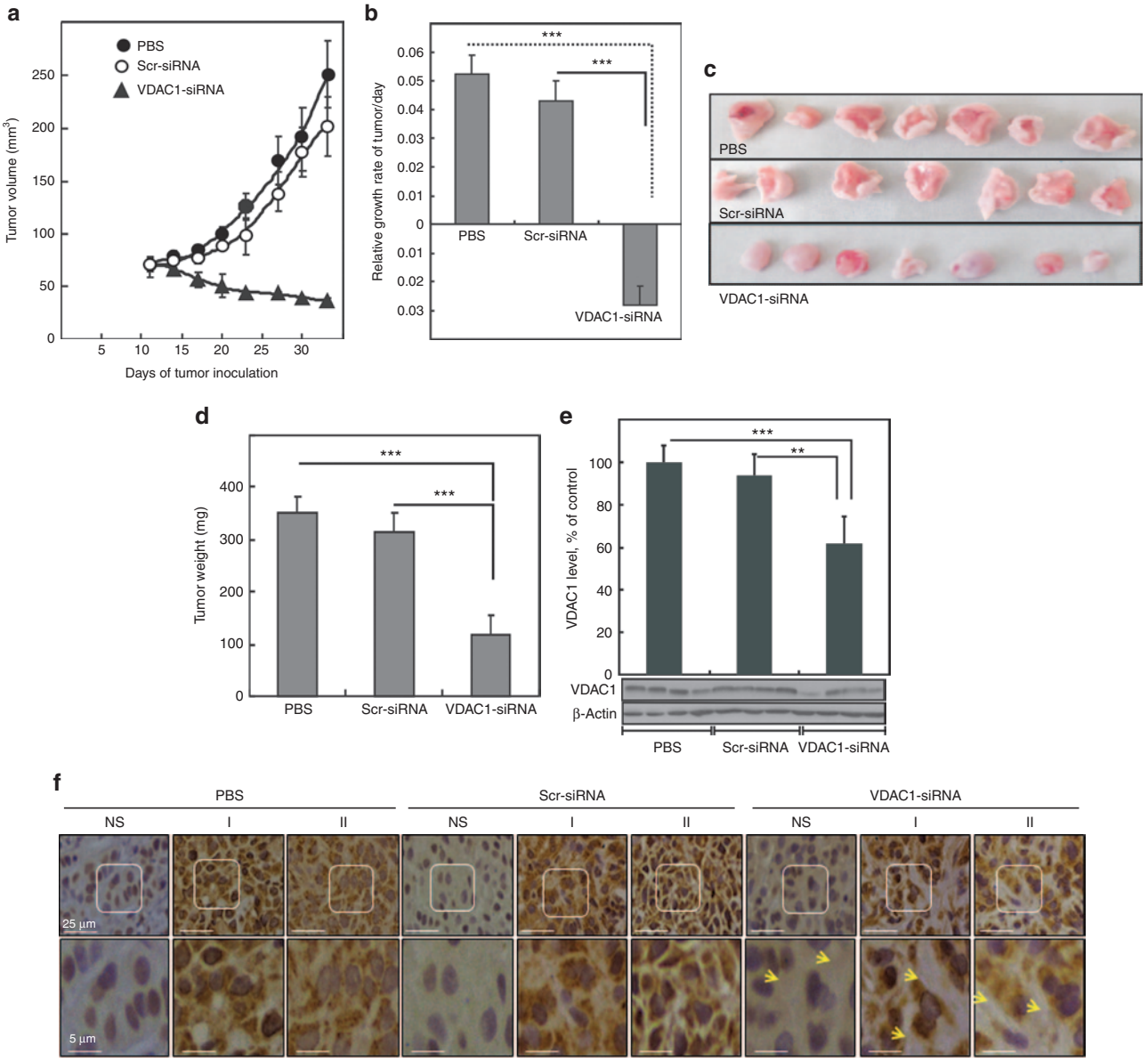

Figure 8 hVDAC1-siRNA inhibits tumor growth and regresses lung cancer xenografts. A549 cells were inoculated into male nude mice (7×10^6 cells/mouse). Tumor volumes were monitored (using a digital caliper) and on day 11, the mice were divided into three groups (8 or 9 mice per group), with each mouse containing a tumor with a volume between 60 and 100 mm^3 and similar average volumes measured per group. The three mice groups were subjected to the following treatments: Xenografts were injected with phosphate-buffered saline ((•), control), with scrambled small interfering RNA (siRNA) (o) (10 µl of a 400 nmol/l solution) or with voltage-dependent anion channel (VDAC1)-siRNA (▲) (10 µl of a 400 nmol/l solution). In **a**, xenograft sizes were measured on the indicated days and the calculated average tumor volumes are presented as means ± SEM, $^{***}P < 0.001$. In **b**, one-way repeated measures analysis of variance (ANOVA) indicated that the change in tumor volume over time differed significantly in the three treatment groups (treatment × time of interaction; $F_{14,140} = 17.07$, $^{***}P < 0.001$). The relative rate of growth in tumor volume of each individual was estimated using a nonlinear regression fitted to an exponential model (see Results section). One-way ANOVA indicated significant differences in relative growth rates in the three treatment groups ($F_{2,20} = 42.59$, $^{***}P < 0.001$). Tumors from mouse A549 cell xenografts were dissected (**c**), weighted, and the results were analyzed using the Mann–Whitney *U*-test ($^{**}P < 0.05$) (**d**). in (**e**), Representative immunoblots of VDAC1 expression levels in lysates from xenografts of the four mice from each group and quantitation of their relative VDAC1 expression levels (relative units) are presented ($^{**}P < 0.0284$, $^{***}P < 0.004$). (**f**) Dissected tumors were subjected to immunohistochemistry, carried out as described in the Materials and Methods. Photomicrographs showing immunohistochemical staining of tumor sections from two mice (I and II) from each group with anti-VDAC1 antibodies. Non-specific (NS) represents staining with only secondary antibodies. Arrowheads point to nonstained area. Bars represent 25 µm (5 µm for the enlarged section).

The dramatic inhibition of cell growth by VDAC1-siRNA, particularly in high energy- and metabolite-requiring cancer cells, can be explained by the important function of VDAC1 in energy production through its control of trafficking of ATP/ADP, NADH/NAD, and many other metabolites into and out of the intermitochondrial membrane space.[8,18–20] This is clearly reflected in the overexpression of VDAC1 in various cancer cell lines (**Figure 4e**). This is further evident when

comparing VDAC1 expression in healthy and tumor lung tissues from the same patient, where an overexpression of up to eightfold higher is seen in the tumor tissue (**Figure 4f**). Similar findings were reported previously with the higher expression of VDAC1 and its C-terminal truncated form being increased with lung cancer stage.[32] Indeed, cell treatment with VDAC1-siRNA resulted in a decrease in cell energy production (**Figure 5**), as also reflected in the decrease in succinate dehydrogenase activity within the mitochondria, as analyzed using the XTT assay (**Figure 4d**), and with tight correlation between cell growth and cellular ATP levels being seen.[21]

Mitochondria depleted of VDAC1 with a limited source of metabolites should act inefficiently, leading to increased ROS production.[33] This prediction is supported by the findings that both cytosolic and mitochondrial ROS levels increased upon VDAC1 silencing, in comparison to ROS levels in VDAC1-expressing cells, although the observed increase is only about 10% of the level produced by cells treated with As_2O_3 or rotenone (**Figure 5c–e**).

In this respect, a significant correlation was found between the expression of VDAC and the induction of H_2O_2 production and cell death elicited by Furanonaphthoquinones in several human cancer cell lines.[34] Thus, the cell growth inhibition caused by VDAC1-siRNA due to impaired metabolic and energy homeostasis is further amplified by ROS production.

In tumor cells, ATP production is more dependent on glycolysis than on mitochondrial respiration, an observation termed the Warburg effect.[35,36] Recent reports revealed that inhibiting tumor cell glycolysis efficiently suppressed tumor cell malignancies, such as tumor cell invasion and proliferation.[37,38] *In vitro* wound-healing assays designed to study cell migration define the degree of the invasive behavior of cancer cells.[39,40] Here, we demonstrated that A549 lung cancer cells silenced for VDAC1 expression have low migration capacity even when chemotactically stimulated by bFGF, a reagent that efficiently enhanced cell migration (**Figure 6**). Thus, inhibited cancer cell migration in VDAC1 expression-silenced cells points to another advantage for the VDAC1-deletion strategy, namely not only the inhibition of tumor development but also cell migration and the subsequent metastasis development.

hVDAC1-siRNA inhibits cancer cell proliferation *in vivo* and its potential use for lung cancers therapy

Considering the impact of a single hVDAC1-siRNA, the low concentration used, the specificity for cancer cells, as well as the long-lasting growth inhibition effect of about 6 days by a single transfection and its extension by 5 days upon a second transfection, and the use of VDAC1-siRNA to inhibit cancer cell growth offers a promising approach for cancer therapy. Accordingly, the impact of VDAC1 silencing *in vivo*, using a Matrigel-based assay providing close to physiological conditions was explored. The Matrigel-based results demonstrated that hVDAC1-siRNA–transfected HepG2 cells showed a dramatic decrease in proliferation rate, in comparison to VDAC1-expressing cells (**Figure 7a,b**).

Since siRNA is easily degraded enzymatically, chemical modifications[26] were introduced in the VDAC1-siRNA to improve *in vivo* stability. An additional benefit of methylation of the ribose 2′-hydroxyl group, in particular, is a diminishing of immune-stimulatory effects.[41] The three 2′OMe-siRNA tested highly inhibited both VDAC1 expression and cell growth (**Figure 7c,d**). As such, hVDAC1-siRNA modified at 6 of its 19 nucleotides was selected for *in vivo* studies (**Figure 8**).

Lung cancer tumor xenografts grown in immunocompromised mice were used to demonstrate the effectiveness of hVDAC1-siRNA in inhibiting tumor growth *in vivo*. The results clearly demonstrate that administration of hVDAC1-siRNA to the A549 cells derived, established xenograft tumor inhibiting its development (**Figure 8**). Strikingly, hVDAC1-siRNA not only inhibited tumor growth but also reduced the size of the tumor to less than half of its original size as measured before starting such treatment, pointing to regression of the established tumor. Furthermore, while PBS- and scrambled siRNA-treated xenograft tumor sections were homogenous with respect to staining with anti-VDAC1 antibodies, the remaining tumor in the VDAC1-siRNA-treated xenografts contains cells stained with anti-VDAC1 antibodies as do the PBS- and scrambled siRNA-treated xenografts, yet also present significant nonstained areas composed of cells distinct from the stained tumor cells, possibly representing cells of mouse origin (**Figure 8f**). Thus, the tumor, in part, contains noncancerous cells. Taken together, these results indicate that tumor treatment with VDAC1-siRNA dramatically prevented tumor growth and reduced the size of the original tumor by over 80% when treated for 20 days.

Due to its high incidence and mortality, lung cancer is the leading cause of cancer deaths worldwide, with 5-year survival rates being less than 10% for non-small cell lung carcinomas diagnosed in advanced stages.[42] Our preclinical lung cancer mouse model results thus clearly point to VDAC1 silencing by VDAC1-siRNA as holding great promise as a novel antilung cancer drug. Despite the promise RNAi offers in terms of cancer therapy,[26] hurdles related to delivery must be overcome before small RNAs can be brought into the clinic.[2,5] With this in mind, recently developed local administration techniques involving delivery agents protecting the siRNA from enzymatic degradation have been described.[2,5,42–44] Such approaches, associated with negligible toxicity, were developed for pulmonary delivery of siRNA, including nonviral therapeutic aerosol bioengineering and nonviral siRNA delivery platforms for delivery via inhalation.[44] Introduced intranasally or by inhalation, siRNAs designed for the treatment of various lung viral infections and other respiratory disorders are currently in phase 2 clinical trials.[43,44] These approaches might also prove of use for hVDAC1-siRNA targeting lung cancer when introduced via appropriate delivery systems, such as lipid- and polymer-based vectors, formulated for inhalation.[45,46]

In summary, one of the hallmarks of cancer is the reprogramming of energy metabolism, a process essential for tumor progression. VDAC1 is an important element of the cellular metabolic and energy homeostasis systems, such that its deletion by specific siRNA alters the normal functioning of cancer cells, leading to growth arrest, as demonstrated in this study. A single hVDAC1-siRNA at low nanomolar concentrations was shown to silence VDAC1 expression and inhibit the growth of various cancer cell types, both *in vitro* and *in vivo*. hVDAC1-siRNA not only inhibited tumor growth but also resulted in regression of an existing tumor. Depletion

of VDAC1 also resulted in inhibition of cancer cell migration and thus could prevent metastasis formation. Considering the high expression level of VDAC1 in cancer cells and the specificity of VDAC1-siRNA for the inhibition of cancer cell and tumor growth, silencing VDAC1 expression can be considered as a novel therapeutic approach to treat cancer.

Materials and methods

Materials. The cell transfection agents, JetPRIME and Jet-PEI, were from PolyPlus transfection (Illkirch, France), while siRNA came from Dharmacon (Lafayette, CO). Vybrant DiD cell-labeling solution was obtained from Invitrogen (Grand Island, NY). BD Matrigel and a BrdU Flow BD Pharmingen kit were purchased from BD Biosciences (Franklin Lakes, NJ). Carbonyl cyanide 4-(trifluoromethoxy)phenylhydrazone (FCCP), 2′,7′-dichlorofluorescin diacetate (DCFDA), leupeptine, phenylmethylsulfonylfluoride, sulforhodamine B (SRB), tetramethylrhodamine methylester (TMRM), and recombinant basic fibroblast growth factor (bFGF) were obtained from Sigma (St Louis, MO). Rabbit polyclonal antibodies against VDAC1 amino acids 150–250 came from Abcam (Cambridge, UK). Monoclonal anti-actin antibodies were obtained from Santa Cruz Biotechnology (Santa Cruz, CA), while horseradish peroxidase-conjugated goat anti-mouse and anti-rabbit antibodies were obtained from Promega (Madison, WI). Dulbecco's modified Eagle's medium, RPMI 1640 and Hank's balanced salt solution growth media, normal goat serum and the supplements fetal calf serum, L-glutamine, penicillin-streptomycin, and 2,3-Bis-(2-Methoxy-4-Nitro-5-Sulfophenyl)-2*H*-Tetrazolium-5-Carboxanilide, (XTT) reagent were obtained from Biological Industries (Beit Haemek, Israel). MitoSOX Red was obtained from Invitrogen.

Cell culture. HepG2 (human hepatocellular carcinoma), HCT116 (human colorectal carcinoma), HEK293, HeLa (human cervical adenocarcinoma), H358 (human non-small cell lung cancer), A549 (human lung adenocarcinoma epithelial cell, non-small human lung carcinoma), HaCaT (human keratinocyte), MIN-6 (pancreatic cells), and Panc-1 (human pancreatic carcinoma) cells were maintained in Dulbecco's modified Eagle's medium supplemented with 10% fetal calf serum, 2 mmol/l L-glutamine, 1,000 U/ml penicillin, and 1 mg/ml streptomycin. PC3 (prostate cancer) and U-87 (human glioblastoma carcinoma) cells were maintained in RPMI 1640 supplemented with 10–20% fetal calf serum, 2 mmol/l L-glutamine, 1,000 U/ml penicillin, and 1 mg/ml streptomycin. All cells were incubated at 37 °C in 5% CO_2.

Tissue samples. Eleven patients that underwent lobectomy provided lung tissue samples were obtained in accordance with an Institutional Review Board and using protocol approved by the Ethics Committee of the Soroka University Medical Center. The patients received the necessary information concerning the study, and consent was obtained. Fresh paired healthy and cancer tissues from the same lung cancer patient were frozen in liquid nitrogen immediately after surgical removal and maintained at –80 °C until use for western blot analysis. All human tissues were collected with the understanding and written consent of each subject, and the study methodologies conformed to the standards set by the Declaration of Helsinki.

siRNA and cell transfection. Nonmodified and 2′-O-methyl-modified hVDAC1-siRNAs were synthesized by Dharmacon or were obtained from Genepharma (Suzhou, China). The following sequences (names underlined) were used, with 2′-O-methyl-modified nucleotides indicated in bold and underlined (nucleotide positions are provided for sense (S) and antisense (AS) sequences): si-hVDAC1-S:238-5′ACACUAGGCACCGAGAUUA3′-256 and AS: 5′UAAUCUCGGUGCCUAGUGU3′; si-hVDAC1 1/A- S: -238-5′ACAC**U**AG**G**CACCGAGA**U**UA 3′- 256, and AS: 5′UAA UC**U**CGGUGCCUA**G**UGU3′-256; si-hVDAC1 2/A- S: 238-5′ ACAC**U**AG**G**CACC**G**AGA**U**UA3′-256 and AS: 238-5′UAAUC**U** CGGUGCCUA**G**UGU3′; si-hVDAC1 2/B-, S: 238-5′ACAC**U**AG **G**CACC**G**AGA **U**UA3′-256 and AS: 238-5′UAAUC**U**CGG **U**GCCUA**G**UGU3′-256; si-mVDAC1- S: 238-5′ACCCUGGG CACUGAGAUCA3′-256 and AS: 238-5′UGAUCUCAGUGCCC AGGGU 3′-256; and Scrambled- S: -5′GCAAACA**U**CCCA**G**AG G**U**AU3′ and AS : -5′AUACC**U**CUGG**G**AUGUUUGC3′.

Cells were seeded (150,000 cells/well) on six-well culture dishes to 30–50% confluence and transfected with 5–100 nmol/l siRNA-hVDAC1 using the JetPRIME reagent in the case of HeLa and A549, PC-3, HepG2, U87, HaCat, and Min-6 and Panc-1cells, while HCT116 and HEK293, cells were transfected using Dharmafect, all according to the manufacturers' instructions.

Quantitative real-time PCR (RT-PCR) analysis. Total RNA was isolated from A549 cells not treated or treated with scrambled- or VDAC1-siRNA using the RNeasy Mini kit (Qiagen, Valencia, CA) as described by the manufacturer. Complementary DNA was synthesized from 1 µg total RNA using the high-capacity cDNA reverse transcription kit with RNase inhibitor and random hexamer primers (Applied Biosystems, Foster City, CA). Real-time qPCR analysis of cDNA was performed in triplicate using TaqMan master mix and TaqMan specific probes and primers for VDAC1 (Hs01631624_gH), VDAC2 (Hs00748551_s1), and VDAC3 (Hs01091534_g1). The levels of the target genes were normalized relative to hypoxanthine phosphoribosyltransferase 1 (HPRT1) (Hs99999909_m1) and TATA box-binding protein (Hs99999910_m1) mRNA levels. Samples were amplified in a 7300 Real Time PCR System (Applied Biosystems) for 40 cycles using the following PCR parameters: 95 °C for 15 seconds, 60 °C for 1 minute, and 72 °C for 1 minute. The mean fold changes (± SEM) of the three replicates were calculated.

SRB assay for cell proliferation and XTT for mitochondrial succinate dehydrogenase activity. Cells 24 hours post-transfection with scrambled or hVDAC1-siRNA were counted and seeded in 96-well plates. After an additional 24, 48, 72, 96, 120, or 144 hours, the cells were washed twice with PBS, fixed with 10% trichloroacetic acid (TCA) for 1–2 hours, and subsequently stained with SRB. SRB was extracted from the cells using 100 mmol/l Tris base, and absorbance at 510 nm was determined using a plate reader (Tecan Trading, Männedorf, Switzerland). The XTT assay was performed according to the manufacturer's protocol.

Mitochondrial membrane potential determination. Mitochondrial membrane potential ($\Delta\Psi$) was determined using TMRM dye. HepG2, A549, and PC-3 cells were transfected with scrambled or hVDAC1-siRNA, and 48 hours post-transfection, the cells were incubated with TMRM (500 nmol/l, 30 minutes) and washed twice with PBS. TMRM fluorescence was measured with a plate reader. FCCP served as a control for $\Delta\Psi$ dissipation.

Determination of cellular ATP levels. Cellular ATP levels were estimated using the luciferase-based assay (CellTiter-Glo; Promega). Cells were transfected with scrambled- or hVDAC1-siRNA, and 36 hours post-transfection, the cells were washed twice with PBS and seeded in 96-well plates at densities of 5×10^4 cells/ml (A549 and HepG2 cells) or 7×10^4 cells/ml (PC-3 cells). ATP levels were assayed according to the manufacturer's protocol, and luminescence was recorded using an Infinite M1000 plate reader (Tecan Trading, Manedorf, Switzerland). ATP levels were calculated in relation to protein, as determined in parallel by the SRB assay.

Measurement of superoxide generation. ROS production was monitored using the oxidant sensitive dye DCFDA fluorescent probe, a cell-permeable indicator of ROS, which is converted by H_2O_2 and peroxidases to the DCF fluorescent derivate. Briefly, cells were washed once with serum- and phenol red–free medium and then incubated with DCFDA 4 μmol/l) for 30 minutes. For mitochondrial accumulated ROS, MitoSOX Red)4 μmol/l), mitochondrial superoxide indicator for live-cell imaging was used according to the manufacturer's protocol. Fluorescence was measured using a FACscan flow cytometer (BD Biosciences, Franklin Lakes, NJ) and analyzed using Cell Quest software (BD Biosciences).

Colony-forming assay. Cells were transfected with scrambled- or VDAC1-siRNA, and 24 hours post-transfection, the cells were seeded in six-well plates at a density of 3,000 cells/well and incubated for 96 hours at 37 °C in a humidified atmosphere of 5% CO_2. The medium was decanted and the colonies were fixed with 4% (v/v) paraformaldehyde at room temperature for 10 minutes, and stained with 0.1% crystal violet (in 95% ethanol) for 30 minutes for colony visualization. Plates were then washed with water, dried, and imaged using Image J software for colony number counting.

Gel electrophoresis and immunoblotting. Sodium dodecyl sulfate–polyacrylamide gel electrophoresis was performed according to the Laemmli protocol.[47] For immunoblotting with anti-VDAC1 antibodies, membranes containing electrotransferred proteins were incubated with a blocking solution containing 5% nonfat dry milk and 0.1% Tween-20 in Tris-buffered saline, followed by incubation with polyclonal anti-VDAC1 antibodies (1:4,000). Membranes were then incubated with horseradish peroxidase-conjugated anti-rabbit IgG (1:40,000) as secondary antibodies. Antibody binding was detected using an enhanced chemiluminescent substrate (EZ-ECL kit; Biological Industries Israel, Beit-Haemek, Israel). Densitometric quantification of band intensity was performed using Multi-Gauge software (Fujifilm, Tokyo, Japan).

Immunohistochemistry. For immunohistochemistry, formalin-fixed and paraffin-embedded tumor samples were, according to established protocols, sectioned, deparaffinized, and pretreated in antigen retrieval citrate–based solution and heated at 97 °C for 10 minutes. Sections were incubated with anti-VDAC1 antibodies followed by incubation with horseradish peroxidase-conjugated anti-rabbit antibodies and diaminobenzidine. Slides were also hematoxylin-stained and mounted on glass slides with mounting medium. Samples were visualized by confocal microscopy (I×81 motorized inverted microscope; Olympus).

In vitro migration and wound-healing assay. The migration of A549 cells was assayed using the wound-healing assay. Cells were transfected with scrambled- or VDAC1-siRNA, and 24 hours post-transfection, the cells were seeded in 24-well plates and grown to 95–100% confluence. Thereafter, a 200-μl sterile tip was used to scratch a fixed-width band in the cell monolayer. This step was followed by 12–16 hours incubation with medium containing 1% fetal calf serum in the absence or presence of bFGF. Wound closure was monitored using a digital camera mounted on a microscope to follow the position of the migrating front at defined times.

Matrigel plug formation in nude mice. HepG2 cells transfected with hVDAC1-siRNA and control nontransfected cells were stained with Vybrant DiD cell-labeling solution and subsequently mixed with liquid Matrigel at 4 °C. The cell-Matrigel mixture was s.c. injected into the interscapular region of nude mice to form plugs upon increased temperature (37 °C).[48] The mice were exposed to BrdU in the drinking water to label proliferating cells in both the murine host and in the implanted HepG2 cell-containing plug.[1,49] Cells in the Matrigel plugs remained in the mice for 6 days, after which the mice were sacrificed, the plugs were removed, and the cells in the plug were extracted by enzymatic digestion with a solution containing DNase, collagenase, and hyaloronidase in Hank's balanced salt solution. The cells were counted using a hemocytometer and sorted in terms of cells labeled with both DiD and BrdU (cancer cells) and cells labeled only with BrdU (mouse cells) by FACS (BrdU Flow BD Pharmingen kit). Proliferation was analyzed by a FACScan flow cytometer using Cell Quest software.

Xenograft experiments using nude mice. Athymic 8-week-old male SCID nude mice (weight ~15 g) were obtained from Harlan and allowed a week of acclimatization to their new surroundings. A549 lung cancer cells (7×10^7) were injected s.c. into the hind leg flanks of the mice. Approval for the experimental protocol was obtained from the Institutional Animal Care and Use Committee of the Soroka University Medical Center. Eleven days after inoculation, the developing tumors were measured in two dimensions with a digital caliper and tumor volume was calculated as follows: volume = $X^2 \times Y/2$, where X and Y are the short and long tumor dimensions, respectively. The mice with xenografts reaching a volume of 65–100 mm^3 were randomized for different treatments (eight or nine animals in each group): PBS, nontargeting (scrambled) siRNA or modified hVDAC1-siRNA (si-hVDAC1 2/A). Each treatment substance was injected into the established s.c. tumors using the jetPEI delivery reagent (10-μg siRNA/20-μl jetPEI). The xenografts were injected (20 μl per tumor) with PBS or the appropriate siRNA every 3 days.

Beginning on the day of inoculation, mouse weight and tumor volume were monitored twice a week for a period of 33 days using a digital caliper. At the end point of the experiment, *i.e.*, when tumor volume reached ~250 mm^3, the mice were sacrificed using CO_2 gas; the tumors were excised and *ex vivo* weight was determined. Half of each tumor was fixed in 4% buffered formaldehyde, paraffin-embedded and processed for histological examination, while the second half was frozen in liquid nitrogen and stored in –80 °C for immunoblot analysis.

Statistical analysis. Data are expressed as means ± SEM. Statistical evaluation was carried out using Student's *t*-test (two-tailed) to test for differences between the control and experimental results. The level of significance of differences between control and treated sample was determined using the nonparametric Mann–Whitney *U*-test. A difference was considered statistically significant when the *P* value was deemed <0.05 (*), <0.01 (**), or <0.001 (***). Tumor volume data were analyzed using one-way repeated measures analysis of variance. In addition, the relative growth rate in tumor volume of each mouse was estimated using a nonlinear regression fitted to an exponential model

$$V_t = V_0 \cdot e^{r \cdot t}$$

where V_0 (mm^3) is the initial tumor volume, *t* is time (in days) and *r* is the relative growth rate (d^{-1}). Differences in the relative growth rates of the three treatment groups were then determined using one-way analysis of variance.

Acknowledgments. This work was supported by a grant from the National Institute for Biotechnology in the Negev, Ben-Gurion University. The support from Phil and Sima Needleman to V.S.-B. is highly acknowledged. The help of Ofer Ovadia in the statistical analysis of the mouse model data and of Eli Aflalo in the histological analysis is highly appreciated.

1. Querbes, W, Bogorad, RL, Moslehi, J, Wong, J, Chan, AY, Bulgakova, E *et al.* (2012). Treatment of erythropoietin deficiency in mice with systemically administered siRNA. *Blood* **120**: 1916–1922.
2. Petrocca, F and Lieberman, J (2011). Promise and challenge of RNA interference-based therapy for cancer. *J Clin Oncol* **29**: 747–754.
3. Soutschek, J, Akinc, A, Bramlage, B, Charisse, K, Constien, R, Donoghue, M *et al.* (2004). Therapeutic silencing of an endogenous gene by systemic administration of modified siRNAs. *Nature* **432**: 173–178.
4. Jagani, H, Rao, JV, Palanimuthu, VR, Hariharapura, RC and Gang, S (2013). A nanoformulation of siRNA and its role in cancer therapy: *in vitro* and *in vivo* evaluation. *Cell Mol Biol Lett* **18**: 120–136.
5. de Fougerolles, A, Vornlocher, HP, Maraganore, J and Lieberman, J (2007). Interfering with disease: a progress report on siRNA-based therapeutics. *Nat Rev Drug Discov* **6**: 443–453.
6. Ye, QF, Zhang, YC, Peng, XQ, Long, Z, Ming, YZ and He, LY (2012). Silencing Notch-1 induces apoptosis and increases the chemosensitivity of prostate cancer cells to docetaxel through Bcl-2 and Bax. *Oncol Lett* **3**: 879–884.
7. Bai, Z, Zhang, Z, Qu, X, Han, W and Ma, X (2012). Sensitization of breast cancer cells to taxol by inhibition of taxol resistance gene 1. *Oncol Lett* **3**: 135–140.
8. Shoshan-Barmatz, V, De Pinto, V, Zweckstetter, M, Raviv, Z, Keinan, N and Arbel, N (2010). VDAC, a multi-functional mitochondrial protein regulating cell life and death. *Mol Aspects Med* **31**: 227–285.
9. Gincel, D, Zaid, H and Shoshan-Barmatz, V (2001). Calcium binding and translocation by the voltage-dependent anion channel: a possible regulatory mechanism in mitochondrial function. *Biochem J* **358**(Pt 1): 147–155.
10. Keinan, N, Pahima, H, Ben-Hail, D and Shoshan-Barmatz, V (2013). The role of calcium in VDAC1 oligomerization and mitochondria-mediated apoptosis. *Biochim Biophys Acta* **1833**: 1745–1754.
11. Hajnóczky, G and Csordás, G (2010). Calcium signalling: fishing out molecules of mitochondrial calcium transport. *Curr Biol* **20**: R888–R891.
12. Decuypere, JP, Monaco, G, Missiaen, L, De Smedt, H, Parys, JB and Bultynck, G (2011). IP(3) Receptors, Mitochondria, and Ca Signaling: Implications for Aging. *J Aging Res* **2011**: 920178.
13. Huang, H, Hu, X, Eno, CO, Zhao, G, Li, C and White, C (2013). An interaction between Bcl-xL and the voltage-dependent anion channel (VDAC) promotes mitochondrial Ca2+ uptake. *J Biol Chem* **288**: 19870–19881.
14. Rone, MB, Fan, J and Papadopoulos, V (2009). Cholesterol transport in steroid biosynthesis: role of protein-protein interactions and implications in disease states. *Biochim Biophys Acta* **1791**: 646–658.
15. Campbell, AM and Chan, SH (2008). Mitochondrial membrane cholesterol, the voltage dependent anion channel (VDAC), and the Warburg effect. *J Bioenerg Biomembr* **40**: 193–197.
16. Fang, L, Choi, SH, Baek, JS, Liu, C, Almazan, F, Ulrich, F *et al.* (2013). Control of angiogenesis by AIBP-mediated cholesterol efflux. *Nature* **498**: 118–122.
17. Kuznetsov, AV, Javadov, S, Guzun, R, Grimm, M and Saks, V (2013). Cytoskeleton and regulation of mitochondrial function: the role of beta-tubulin II. *Front Physiol* **4**: 82.
18. Lemasters, JJ and Holmuhamedov, E (2006). Voltage-dependent anion channel (VDAC) as mitochondrial governator–thinking outside the box. *Biochim Biophys Acta* **1762**: 181–190.
19. Shoshan-Barmatz, V and Mizrachi, D (2012). VDAC1: from structure to cancer therapy. *Front Oncol* **2**: 164.
20. Shoshan-Barmatz, V and Golan, M (2012). Mitochondrial VDAC1: function in cell life and death and a target for cancer therapy. *Curr Med Chem* **19**: 714–735.
21. Abu-Hamad, S, Sivan, S and Shoshan-Barmatz, V (2006). The expression level of the voltage-dependent anion channel controls life and death of the cell. *Proc Natl Acad Sci USA* **103**: 5787–5792.
22. Koren, I, Raviv, Z and Shoshan-Barmatz, V (2010). Downregulation of voltage-dependent anion channel-1 expression by RNA interference prevents cancer cell growth in vivo. *Cancer Biol Ther* **9**: 1046–1052.
23. Sun, L, Shukair, S, Naik, TJ, Moazed, F and Ardehali, H (2008). Glucose phosphorylation and mitochondrial binding are required for the protective effects of hexokinases I and II. *Mol Cell Biol* **28**: 1007–1017.
24. Konson, A, Pradeep, S, D'Acunto, CW and Seger, R (2011). Pigment epithelium-derived factor and its phosphomimetic mutant induce JNK-dependent apoptosis and p38-mediated migration arrest. *J Biol Chem* **286**: 3540–3551.
25. McGee, GS, Davidson, JM, Buckley, A, Sommer, A, Woodward, SC, Aquino, AM *et al.* (1988). Recombinant basic fibroblast growth factor accelerates wound healing. *J Surg Res* **45**: 145–153.
26. Bumcrot, D, Manoharan, M, Koteliansky, V and Sah, DW (2006). RNAi therapeutics: a potential new class of pharmaceutical drugs. *Nat Chem Biol* **2**: 711–719.
27. Giladi, H, Ketzinel-Gilad, M, Rivkin, L, Felig, Y, Nussbaum, O and Galun, E (2003). Small interfering RNA inhibits hepatitis B virus replication in mice. *Mol Ther* **8**: 769–776.
28. Xia, H, Mao, Q, Eliason, SL, Harper, SQ, Martins, IH, Orr, HT *et al.* (2004). RNAi suppresses polyglutamine-induced neurodegeneration in a model of spinocerebellar ataxia. *Nat Med* **10**: 816–820.
29. Judge, AD, Robbins, M, Tavakoli, I, Levi, J, Hu, L, Fronda, A *et al.* (2009). Confirming the RNAi-mediated mechanism of action of siRNA-based cancer therapeutics in mice. *J Clin Invest* **119**: 661–673.
30. Grills, C, Jithesh, PV, Blayney, J, Zhang, SD and Fennell, DA (2011). Gene expression meta-analysis identifies VDAC1 as a predictor of poor outcome in early stage non-small cell lung cancer. *PLoS One* **6**: e14635.
31. Simamura, E, Shimada, H, Hatta, T and Hirai, K (2008). Mitochondrial voltage-dependent anion channels (VDACs) as novel pharmacological targets for anti-cancer agents. *J Bioenerg Biomembr* **40**: 213–217.
32. Brahimi-Horn, MC, Ben-Hail, D, Ilie, M, Gounon, P, Rouleau, M, Hofman, V *et al.* (2012). Expression of a truncated active form of VDAC1 in lung cancer associates with hypoxic cell survival and correlates with progression to chemotherapy resistance. *Cancer Res* **72**: 2140–2150.
33. Azoulay-Zohar, H, Israelson, A, Abu-Hamad, S and Shoshan-Barmatz, V (2004). In self-defence: hexokinase promotes voltage-dependent anion channel closure and prevents mitochondria-mediated apoptotic cell death. *Biochem J* **377**(Pt 2): 347–355.
34. Simamura, E, Hirai, K, Shimada, H, Koyama, J, Niwa, Y and Shimizu, S (2006). Furanonaphthoquinones cause apoptosis of cancer cells by inducing the production of reactive oxygen species by the mitochondrial voltage-dependent anion channel. *Cancer Biol Ther* **5**: 1523–1529.
35. Hsu, PP and Sabatini, DM (2008). Cancer cell metabolism: Warburg and beyond. *Cell* **134**: 703–707.
36. Pedersen, PL (2007). The cancer cell's "power plants" as promising therapeutic targets: an overview. *J Bioenerg Biomembr* **39**: 1–12.
37. Xu, RH, Pelicano, H, Zhou, Y, Carew, JS, Feng, L, Bhalla, KN *et al.* (2005). Inhibition of glycolysis in cancer cells: a novel strategy to overcome drug resistance associated with mitochondrial respiratory defect and hypoxia. *Cancer Res* **65**: 613–621.
38. Beckner, ME, Stracke, ML, Liotta, LA and Schiffmann, E (1990). Glycolysis as primary energy source in tumor cell chemotaxis. *J Natl Cancer Inst* **82**: 1836–1840.
39. Ridley, AJ, Schwartz, MA, Burridge, K, Firtel, RA, Ginsberg, MH, Borisy, G *et al.* (2003). Cell migration: integrating signals from front to back. *Science* **302**: 1704–1709.

40. Lauffenburger, DA and Horwitz, AF (1996). Cell migration: a physically integrated molecular process. *Cell* **84**: 359–369.
41. Sioud, M, Furset, G and Cekaite, L (2007). Suppression of immunostimulatory siRNA-driven innate immune activation by 2'-modified RNAs. *Biochem Biophys Res Commun* **361**: 122–126.
42. Jemal, A, Siegel, R, Xu, J and Ward, E (2010). Cancer statistics, 2010. *CA Cancer J Clin* **60**: 277–300.
43. Merkel, OM and Kissel, T (2012). Nonviral pulmonary delivery of siRNA. *Acc Chem Res* **45**: 961–970.
44. Watts, JK and Corey, DR (2010). Clinical status of duplex RNA. *Bioorg Med Chem Lett* **20**: 3203–3207.
45. Ramsey, JM, Hibbitts, A, Barlow, J, Kelly, C, Sivadas, N and Cryan, SA (2013). 'Smart' non-viral delivery systems for targeted delivery of RNAi to the lungs. *Ther Deliv* **4**: 59–76.
46. Fujita, Y, Takeshita, F, Kuwano, K and Ochiya, T (2013). RNAi Therapeutic Platforms for Lung Diseases. *Pharmaceuticals (Basel)* **6**: 223–250.
47. Laemmli, UK (1970). Cleavage of structural proteins during the assembly of the head of bacteriophage T4. *Nature* **227**: 680–685.
48. Voronov, E, Shouval, DS, Krelin, Y, Cagnano, E, Benharroch, D, Iwakura, Y *et al.* (2003). IL-1 is required for tumor invasiveness and angiogenesis. *Proc Natl Acad Sci USA* **100**: 2645–2650.
49. Tough, DF and Sprent, J (1994). Turnover of naive- and memory-phenotype T cells. *J Exp Med* **179**: 1127–1135.